

Thermal behavior of hafnium-based ultrathin films on silicon

R. P. Pezzi, J. Morais, S. R. Dahmen, K. P. Bastos, L. Miotti, G. V. Soares,
and I. J. R. Baumvol^{a)}

Instituto de Física, UFRGS, Av. Bento Gonçalves 9500, Porto Alegre, RS, Brazil 91509-900

F. L. Freire, Jr.

*Departamento de Física, PUC-RIO, Rua Marquês de São Vicente, 225, Rio de Janeiro, RJ,
Brazil 22452-970*

(Received 25 November 2002; accepted 17 March 2003; published 2 July 2003)

We report here on the thermodynamical stability of ultrathin, hafnium-based dielectric films, namely hafnium oxide (HfO_2), silicate (HfSi_xO_y), and aluminum silicate ($\text{AlHf}_x\text{Si}_y\text{O}_z$), deposited on silicon. These materials are promising candidates to replace the well established silicon oxide and oxynitride as gate dielectric materials in advanced Si-based complementary metal–oxide–semiconductor technology. Since there are mandatory requirements on the gate dielectric material, hafnium oxide is currently being modified, by adding silicon and aluminum into the matrix, increasing its thermal stability, and improving its electrical properties. Diffusion-reaction during thermal processing was investigated using isotopic substitution together with ion beam techniques such as Rutherford backscattering spectrometry, narrow nuclear resonance profiling, and nuclear reaction analysis. The chemical changes in the films were accessed by x-ray photoelectron spectroscopy. © 2003 American Vacuum Society. [DOI: 10.1116/1.1575218]

I. INTRODUCTION

The International Technology Roadmap for Semiconductors¹ foresees that the silicon oxynitride interim solution for gate dielectric can be used for another two to four years. Then, further development in Si-based integrated circuits will rely on the use of alternative materials with dielectric constants much higher than that of silicon oxide or oxynitrides.

Although adequately low leakage currents have been reported for the capacitance equivalent to SiO_2 thickness OET as low as 1 nm and less,^{2,3} there are many aspects that may prevent the introduction of high- k dielectrics in advanced complementary metal–oxide–semiconductor (CMOS) fabrication technology. The first major difficulty comes from the fact that, besides having a dielectric constant substantially higher than that of SiO_2 and SiO_xN_y , any potential candidate for replacement as a gate dielectric must also have a (i) comparable energy band gap, (ii) comparably low ($\sim 10^{10}/\text{cm}^2$) defect charge density, and (iii) comparably low ($\sim 10^{10}/\text{cm}^2 \text{eV}$) density of electronic interface states.⁴ These conditions will be extremely hard to meet, especially condition (iii). For this reason, many recent studies point out that one or a few monolayers of SiO_2 or SiO_xN_y will most probably be thermally grown as an intermediate layer, in order to preserve the outstanding electrical and structural quality of the SiO_2/Si interface.

Furthermore, in order to maintain its integrity, any potential high- k material must be as thermodynamically stable on Si as SiO_2 or SiO_xN_y , which means that in further processing steps following gate dielectric film deposition. (i) The chemical reaction in the bulk and at the high- k dielectric/Si interface⁵ must be prevented, (ii) the oxygen diffusion

through the high k film and oxygen reaction with a Si substrate must be controlled, and (iii) migration and eventual segregation of any element, especially at the electrode/dielectric and dielectric/Si interfaces, must be avoided. The results point out to very few metal oxides combining stability on Si and dielectric constant appreciably higher than SiO_xN_y . Among them, one can mention ZrO_2 , HfO_2 , Al_2O_3 , and Y_2O_3 . One final, very delicate concern is the recrystallization⁴ of the initially amorphous high- k dielectric films, which would lead to a dramatic increase of leakage current due to grain-boundary conduction. Unlike SiO_2 , many metal–oxide films have a strong driving force to crystallize. The addition of either Si or Al to metal–oxide films on Si can eliminate or strongly reduce the crystallization of these films and this practice is assuming an important role in the search for an alternative gate dielectric material.

The aim of this article is to report on atomic transport and chemical reaction processes during high-temperature annealing of hafnium-based high- k dielectrics on Si. As the thicknesses of the dielectric films range from 1 to 10 nm, the probing techniques used to investigate the thermal stability of the films must have high depth resolution and sensitivity. This makes ion beam techniques such as Rutherford backscattering spectrometry (RBS), nuclear reaction analysis (NRA), and narrow nuclear resonance profiling (NNRP)⁶ suitable to infer compositions and atomic distributions of the elements in the ultrathin films, and their behavior upon annealing. To investigate oxygen diffusion in the films, annealing in a low-pressure oxygen atmosphere enriched to 97% in the ^{18}O isotope was performed. This allows us to distinguish between oxygen previously existent in the film from the newly incorporated during annealing,⁶ and also to determine its depth profile by NNRP, using the narrow resonance at 151 keV in the cross section curve of the $^{18}\text{O}(p,\alpha)^{15}\text{N}$ nuclear

^{a)}Electronic address: israel@if.ufrgs.br

reaction. Channeled RBS was used to estimate the oxygen content in the films. To enhance the depth resolution, RBS was also carried out with a highly tilted geometry, with grazing angle detection to estimate the Hf distribution.⁶ The chemical environment of the elements in the films were analyzed by x-ray photoelectron spectroscopy (XPS), excited by Mg $K\alpha$ radiation of 1253.6 eV with a take-off angle of $\theta = 45^\circ$, where not explicitly specified.

II. HAFNIUM DIOXIDE

Atomic composition and transport and chemical reaction studies during annealing in oxygen of polycrystalline ultrathin HfO_2 films (ellipsometric thickness of 5 nm) deposited in Si(001) substrates were studied. The Si wafers were thermally oxynitrided in NO prior to metal-oxide deposition. The starting structure was prepared by the following sequence: HF cleaning of silicon wafers, followed by annealing in NO, and followed by metalorganic chemical vapor deposition (MOCVD) of HfO_2 at 550 °C using Hf-*t*-butoxide and an oxidant gas. The wafers were then subjected to post-deposition rapid thermal annealing (RTA) in Ar: N_2 at 1000 °C for 10 s (Ar annealing), in order to simulate a typical dopant-annealing step. Finally, the wafers were subjected to RTA in O_2 at 800 °C for 10 or 60 s (O_2 annealing), simulating any of the several usual thermal processing steps. This last annealing step was also alternatively performed in 7×10^3 Pa of O_2 , 97% enriched in the ^{18}O isotope ($^{18}\text{O}_2$ annealing). Furthermore, these $^{18}\text{O}_2$ annealings were performed with and without Ar preannealing, aimed at investigating the effects of the two thermal steps separately.

RBS was carried out using 1 MeV He^+ ions in a channeled geometry and detection at 100° with the incidence direction, as shown in the inset of Fig. 1(b). The signals corresponding to particles backscattered by silicon, oxygen, and nitrogen atoms present in samples 1 (open down triangles), 2 (open circles), and 3 (solid triangles), are plotted in Fig. 1(a), together with the hafnium signal in the inset. From the inset of Fig. 1(a), we can conclude that the amount and depth distribution of Hf remain unchanged after annealing, within the depth resolution of the technique. Table I shows the areal densities of Hf and Si (as determined by channeled RBS) and of ^{16}O , ^{18}O , and ^{14}N (as determined by NRA). O_2 annealing for 60 s (sample 3 in Table I) produces an increase on the O-areal density of about 30% with respect to the as-prepared sample (sample 1) and a comparable percentage decrease on the N-areal density. Figure 1(b) shows Si, ^{16}O , and ^{18}O signals in channeled-RBS spectra of $^{18}\text{O}_2$ -annealed samples for 10 s, with and without Ar preannealing (samples 5 and 6 in Table I). One notices the presence of ^{16}O - ^{18}O exchange, which increases with time of annealing in $^{18}\text{O}_2$ and is much larger for samples that were annealed in $^{18}\text{O}_2$ only than for those that were preannealed in Ar.

Excitation curves of the $^{18}\text{O}(p,\alpha)^{15}\text{N}$ nuclear reaction around the resonance at 151 keV ($\Gamma_r = 100$ eV) and ^{18}O profiles (depth resolution of approximately 0.7 nm near the surface) of as-prepared and $^{18}\text{O}_2$ -annealed samples are shown in Fig. 2. The ^{18}O profiles in samples 5 and 7 (preannealing in

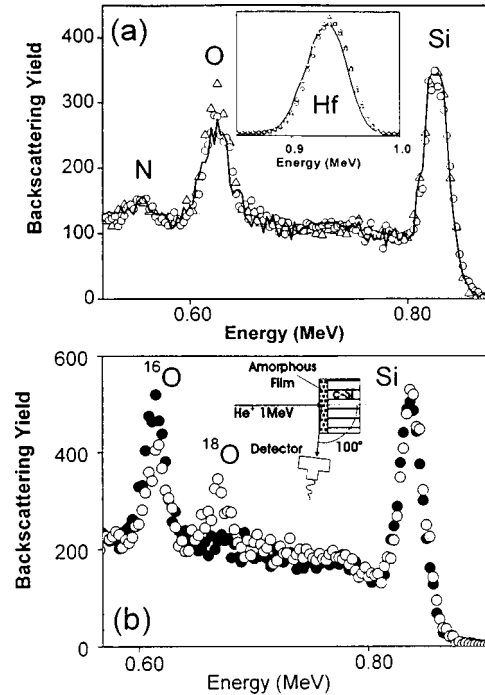


Fig. 1. Channeled-RBS spectra of 1 MeV incident He^+ from HfO_2 films on Si, with detection of the scattered ions at 100° with the direction of incidence. (a) As-prepared sample (solid line), Ar annealing at 1000 °C for 10 s followed by O_2 annealing at 800 °C for 10 s (open circles) and 60 s (triangles). The corresponding Hf signals are shown in the inset (tilted geometry). (b) Ar annealing at 1000 °C for 10 s followed by $^{18}\text{O}_2$ annealing at 800 °C for 10 s (solid circles) and $^{18}\text{O}_2$ annealing only at 800 °C for 10 s (open circles).

Ar+ 10 or 60 s of $^{18}\text{O}_2$ annealing) indicate a propagating ^{18}O front from the surface and reaction (eventually ^{16}O - ^{18}O and N- ^{18}O exchange reactions only) with the HfO_2 network. Furthermore, ^{18}O profiles in samples 6 and 8 ($^{18}\text{O}_2$ annealing only for 10 and 60 s) are deeper and higher. When compared to similar studies performed previously⁷⁻¹¹ in aluminum, zirconium, and gadolinium oxides and silicates, the present $\text{HfO}_2/\text{SiO}_x\text{N}_y$ structure displays higher resistance to oxygen migration from the gas into the solid phase and incorporation therein, as well as smaller isotopic exchanges. ^{29}Si profiles were determined by NNRP (results not shown here), revealing that Si remains immobile during annealing, in contrast to

TABLE I. Areal densities (in units of $10^{15} \times \text{cm}^{-2}$) of different atomic species and isotopes in HfO_2 films on Si. Ar annealing at 1000 °C. Annealings in $^{16}\text{O}_2$ and $^{18}\text{O}_2$ at 800 °C.

Sample	Hf	Si	^{16}O	^{18}O	^{14}N
(1) As prepared	9.5	1.4	22.2	0.02	1.6
(2) Ar + O_2 10 s	9.6	1.4	24.3	0.02	1.5
(3) Ar + O_2 60 s	9.8	1.8	28.5	0.02	1.2
(4) Ar anneal	9.6	1.5	23.2	0.02	1.6
(5) Ar + $^{18}\text{O}_2$ 10 s	9.6	1.5	22.4	0.51	1.5
(6) $^{18}\text{O}_2$ 10 s	9.8	1.7	19.1	6.54	1.4
(7) Ar + $^{18}\text{O}_2$ 60 s	9.5	1.7	22.3	4.76	1.2
(8) $^{18}\text{O}_2$ 60 s	9.6	2.2	15.4	11.13	1.1

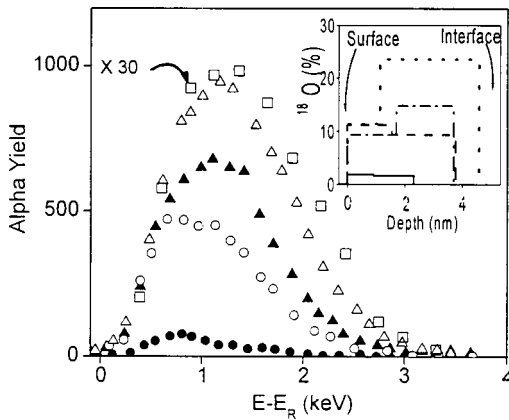


FIG. 2. Excitation curves of the $^{18}\text{O}_2(p, \alpha)^{15}\text{N}$ nuclear reaction around the resonance at 151 keV for HfO_2 films on Si, with the corresponding ^{18}O profiles in the inset: As-prepared sample (sample 1) (open squares, $\times 30$), Ar annealing at 1000 °C for 10 s followed by $^{18}\text{O}_2$ annealing at 800 °C for 10 s (sample 5) (solid circles, solid curve), 60 s (sample 7) (solid triangles, dashed-dotted curve), $^{18}\text{O}_2$ annealing only at 800 °C for 10 s (sample 6) (open circles, dashed curve), and 60 s (sample 8) (open triangles, dotted curve).

several of the earlier mentioned materials where substrate Si is seen to migrate into the oxide film.^{7,9–11}

Figure 3 shows Si $2p$ photoelectron regions for as-prepared and O_2 -annealed (10 and 60 s) samples. The Hf $4f$ and O $1s$ regions for the as-prepared sample are shown in the insets, of Fig. 3, being almost identical to those for the annealed samples. The Si $2p$ region for the starting sample has three components; one around the binding energy of 99.5 eV commonly associated with Si—Si bonds (Si—Si component), another around 103.2 eV associated with different Si—O bonding configurations, including Si—O—Hf bonds (Si—O component),^{2,12} and a third, much smaller component around 101 eV associated with Si in an oxynitride bonding configuration (Si—O—N component).¹² According to literature,^{2,3,12} the Hf $4f$ signal here observed is mostly due to HfO_2 , although minor contributions from Hf—O—Si and Hf—O—N bonds cannot be excluded. Similarly, the O $1s$ signal is attributed² mainly to O—Hf bonds, with a small contribution of O bonded to Si near the interface. The film

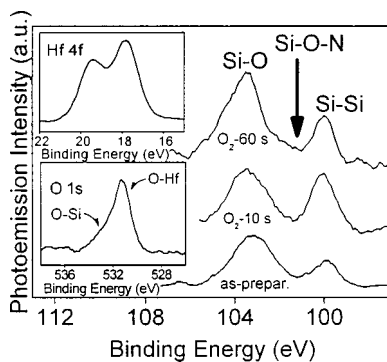


FIG. 3. Si $2p$ photoelectron regions for HfO_2 films on Si: As-prepared sample and for the samples Ar annealed at 1000 °C for 10 s followed by O_2 annealing at 800 °C for 10 and 60 s. The Hf $4f$ and O $1s$ regions for the as-prepared sample are shown in the insets.

composition is then essentially HfO_2 , whereas the interface region has a complex composition, including SiO_2 , SiO_xN_y , SiHf_xO_y (Ref. 13) and $\text{SiHf}_x\text{O}_y\text{N}_z$. The Si—Si/Si—O area ratio increases significantly from the as-prepared to the 10 s O_2 -annealed sample, which could be indicative either of chemical reactions taking place at the interface, or of a higher Si—Si contribution due to the loss of atoms from the $\text{HfO}_2/\text{SiO}_x\text{N}_y$ film. However, this ratio remains constant from the as-deposited to the 60 s O_2 -annealed sample, excluding these possibilities. RBS and NRA data of Table I also exclude $\text{HfO}_2/\text{SiO}_x\text{N}_y$ losses as a possibility. Owing to substantial thinning of the HfO_2 films^{13,14} following Ar annealing, an increase of the Si—Si component contribution from the substrate is expected. The subsequent O_2 annealing for 10 s does not lead a significant amount of oxygen from the gas phase to oxidize Si at the interface (see Figs. 1 and 2 and Table I). Consequently, an increase in the Si—Si/Si—O ratio is observed, as seen in the hafnium silicate, below, and other authors concerning dielectrics containing hafnium. On the other hand, a subsequent 60 s O_2 annealing substantially increases the oxygen content, as well as leads oxygen from the gas phase to reach the interface, oxidizing a Si substrate and thus compensating the increase of the Si—Si component from the substrate due to thinning by a comparable increase of the Si—O component.

The present characterizations indicate an intermediate layer of complex composition between the MOCVD HfO_2 films and the Si substrate, including silicon oxynitride, hafnium silicate, and possibly hafnium—silicon oxynitride. The composition of this structure is essentially stable against Ar preannealing at 1000 °C and O_2 annealing at 800 °C. Oxygen migration proceeds by means of a propagating front from the surface that reacts with the $\text{HfO}_2/\text{SiO}_x\text{N}_y$ network as it advances, the main reaction channels being O—O and O—N exchanges. For the annealing temperatures and times of the present work, the $\text{HfO}_2/\text{SiO}_x\text{N}_y$ structure showed more resistance to O and Si migration and incorporation than others studied previously, with the Ar preannealed samples exhibiting a higher resistance than those directly annealed in O_2 . The intermediate layer is also essentially stable against annealing, apart from moderate N loss due to N—O exchange reaction and SiO_2 formation due to oxidation of the substrate. We attribute this stability to a synergism between the properties of HfO_2 films on Si and the reaction-diffusion barrier constituted by both the SiO_xN_y interlayer and N eventually incorporated into the HfO_2 films.

III. HAFNIUM SILICATE

The hafnium silicate films, which are actually $(\text{HfO}_2)_{1-x}(\text{SiO}_2)_x$ pseudobinary alloys or compounds,^{15,16} were deposited by reactive sputtering in O_2 on HF-cleaned, 200 mm Si(100) p -type substrates. RTA was performed at 1000 °C in N_2 (N_2 annealing) and O_2 (O_2 annealing) at atmospheric pressure. RTA in O_2 was also performed at 1000 °C in 7×10^3 Pa of O_2 97% enriched in the ^{18}O isotope

($^{18}\text{O}_2$ annealing). This allows differentiation between oxygen incorporated from the gas phase and that previously existing in the films.

Cross section high-resolution transmission electron microscopy (HRTEM) images (not shown) revealed that the as-deposited sample consisted of an amorphous $(\text{HfO}_2)_{1-x}(\text{SiO}_2)_x$ layer approximately 3 nm thick and an underlying amorphous SiO_2 -like layer formed on the Si substrate during deposition. HRTEM also indicated that N_2 annealing leads to a densification (thinning) of the $(\text{HfO}_2)_{1-x}(\text{SiO}_2)_x$ layer, and to an increase of the thickness of the SiO_2 layer. The same effects are observed following O_2 annealing, in which case a larger increase of the SiO_2 layer is observed. In all cases, annealing produces an increase in the crystallization of the films.

The 3 nm thick $(\text{HfO}_2)_{1-x}(\text{SiO}_2)_x$ films were also analyzed by angle-resolved XPS. The top of Fig. 4 shows Si $2p$ signals for the as-deposited sample and for N_2 - and O_2 -annealed samples, measured at two different take-off angles between the sample normal and the analyzer axis, namely 60° (surface sensitive mode) and 25° (bulk sensitive mode). The surface sensitive signals were fitted with two components, one associated with Si—O bonds and another correspondent with Si—O—Hf bonds. The ratios between these two components remain approximately constant after annealing. The bulk sensitive signals were fitted with the two aforementioned components plus a third one associated with Si—Si bonds from the substrate. One notices a decrease in the intensity of the Si—Si component with respect to the Si—O and Si—O—Hf components in the sample annealed in O_2 , owing to the increase in thickness of the interlayer as corroborated by HRTEM. This increase in thickness may be due either to the formation of SiO_2 or, eventually, of additional hafnium silicate. The bottom of Fig. 4 shows the O $1s$ signals, which can be fitted with two components, one associated with O—Si bonds and another associated with O—Hf bonds. The strong increase in the intensity of the O—Hf component with respect to the O—Si component in the bulk-sensitive signal of the O_2 -annealed sample shows that the compound responsible for the increase of the interlayer thickness was a silicate rather than SiO_2 .

Elemental composition of the as-deposited samples was determined by RBS and NRA to be approximately HfSi_2O_5 , which remained essentially the same after 60 s RTA at 1000°C in N_2 and O_2 . Channeled-RBS spectra of 1 MeV incident He^+ ions from the as-deposited and N_2 - and O_2 -annealed samples are shown in Fig. 5, evidencing that annealing in N_2 leads to a slight increase in the areal density of oxygen of the samples, while annealing in O_2 leads to a substantial increase in the oxygen areal density. The Hf signal is shown in the inset of Fig. 5(a), using the tilted geometry, where one notices the immobility of Hf within the depth resolution.

$^{18}\text{O}_2$ annealing of the samples shown in Fig. 5(a) leads to the channeled-RBS spectra shown in Fig. 5(b). One notices the incorporation of ^{18}O from the gas phase into the $(\text{HfO}_2)_{1-x}(\text{SiO}_2)_x/\text{SiO}_2$ film structure.

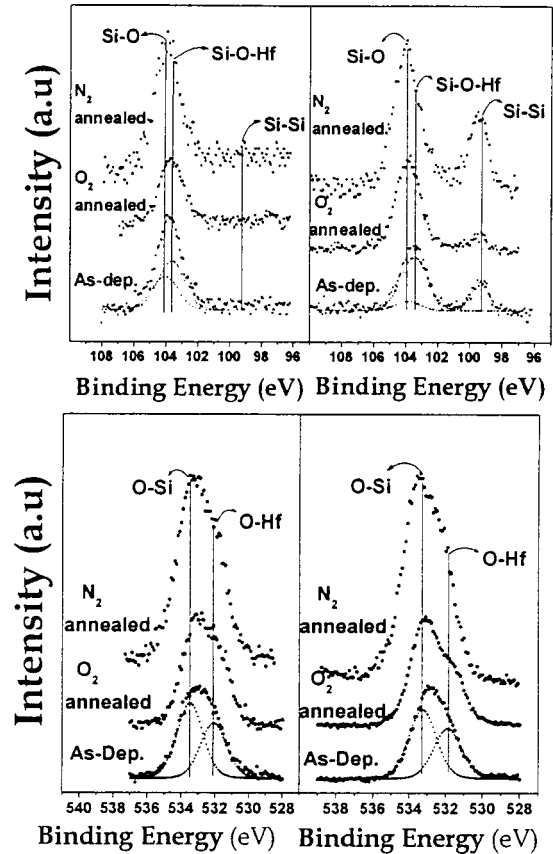


FIG. 4. (Top)—Si $2p$ photoelectron spectra in surface sensitive (left-hand side, take-off angle $\theta=60^\circ$) and bulk sensitive (right-hand side, take-off angle $\theta=25^\circ$) from as-deposited, vacuum, and O_2 -annealed hafnium-silicate films on Si. (Bottom)—The corresponding O $1s$ photoelectrons.

^{18}O profiles in these hafnium silicate film samples were determined by NRP as just discussed. The oxygen front from the gas phase diffuses from the surface reacting with the hafnium-silicate network. Samples that were preannealed in either O_2 or N_2 are more resistant to the propagation of the ^{18}O front than the as-deposited one. Therefore, less ^{18}O will reach and oxidize the Si substrate in the preannealed samples than in the as-deposited one. ^{29}Si profiles were determined for the O_2 -annealed samples using the $^{29}\text{Si}(p,\gamma)^{30}\text{P}$ nuclear reaction around the resonance at 414 keV ($\Gamma=100$ eV). Excitation curves and extracted profiles are shown in Fig. 6. In the bulk of the as-deposited samples, a roughly constant Si concentration is observed, which remained essentially immobile during 1000°C annealing. There is no observable transport of Si from the substrate into the HfSi_xO_y films after annealing, revealing high stability of the bulk and interface regions in contrast with several previously studied materials such as Al_2O_3 , ZrO_2 , Zr-Si-O , and Zr-Al-O .⁷⁻¹³

In the particular case of HfSi_xO_y films on Si studied here, good stability and integrity were observed when they are submitted to RTA at 1000°C , especially if we consider that 30 s of RTA processing is more than enough for most dopant-annealing processing steps. Preannealing in a nonreactive atmosphere like N_2 increases the stability and

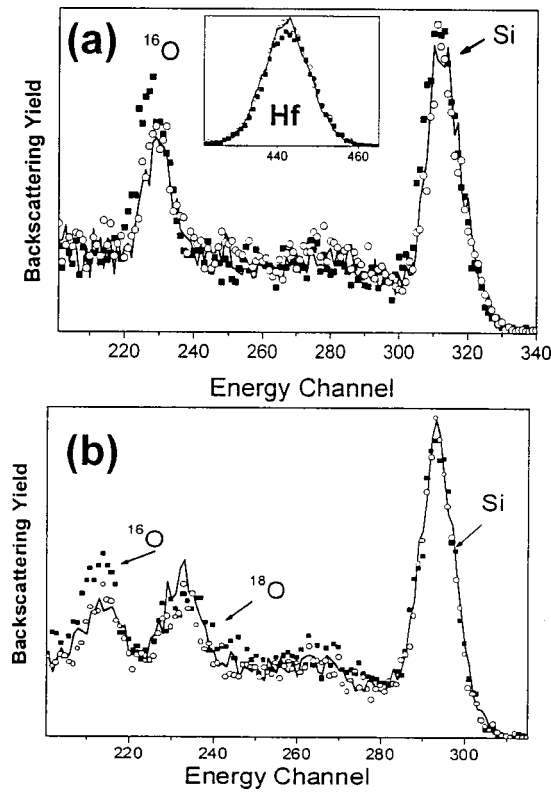


FIG. 5. Channeled-RBS spectra of 1 MeV incident He⁺ ions from hafnium-silicate films on Si (a) as-deposited (solid line) and after annealing in N₂ (open circles) and O₂ (solid circles) at 1000 °C for 60 s and (b) the same samples as in (a), after a second processing step, RTA in ¹⁸O₂ at 1000 °C for 60 s.

resistance to oxidation of the films. Annealing in an oxygen-containing atmosphere reveals a rapidly propagating front of oxygen from the film surface, which reacts with the (HfO₂)_{1-x}(SiO₂)_x network as it advances. When compared to previous materials considered for SiO₂ replacements as gate dielectric, such as Al₂O₃, ZrO₂, Zr-Si-O, Zr-Al-O,

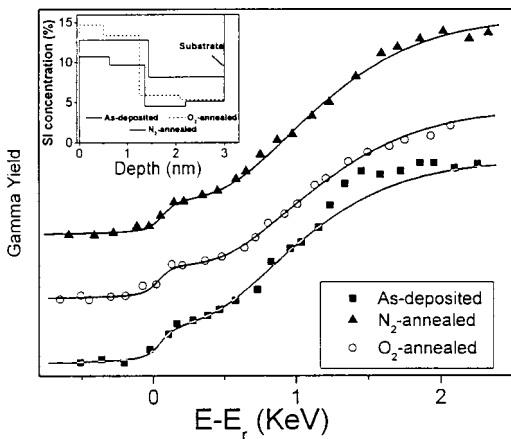


FIG. 6. Excitation curves of the ²⁹Si(*p*, γ)³⁰P nuclear reaction around the resonance at 414 keV with the corresponding ²⁹Si profiles in the inset from (HfO₂)_{1-x}(SiO₂)_x on Si, as-deposited (squares), N₂-annealed (triangles), and O₂-annealed (circles) samples. The curves are shifted to improve clarity.

TABLE II. Annealing parameters for AlHf_xSi_yO_z films, performed in 7 × 10³ Pa of O₂ enriched to 97% in the ¹⁸O isotope (¹⁸O₂), with the corresponding areal densities of Hf, ¹⁸O, and ¹⁶O present in the films, in units of 10¹⁵ × cm⁻².

Sample	Temperature	Time	Hf	¹⁸ O	¹⁶ O
1	as deposited	...	4.79	...	24.75
2	600 °C	30 s	4.72	0.65	24.92
3	600 °C	90 s	4.61	1.31	25.84
4	600 °C	180 s	5.06	1.71	26.00
5	800 °C	60 s	4.88	1.78	24.33
6	800 °C	90 s	4.29	1.90	23.56
7	800 °C	180 s	5.03	5.94	21.60
8	1000 °C	spike	4.94	17.64	21.61
9	1000 °C	10 s	4.55	12.10	21.48
10	1000 °C	20 s	3.87	10.94	21.13

Gd₂O₃, Gd-Si-O, and others, the hafnium silicate films present higher stability under annealing at 1000 °C.

IV. HAFNIUM ALUMINUM SILICATE

The AlHf_xSi_yO_z films were deposited by reactive sputtering, using a HfO₂ target partially covered with pieces of aluminum and silicon. In order to observe the behavior of the material when different processing parameters are varied, the as-deposited, 3.5 nm thick AlHf_xSi_yO_z films were submitted to nine different annealing conditions in ¹⁸O₂, maintaining the same ¹⁸O₂ pressure, as shown in Table II, which includes a spike annealing at 1000 °C.

Figure 7 shows channeled-RBS spectra of the as-deposited and annealed (10 s at 1000 °C) samples, where one can clearly notice the incorporation of ¹⁸O in the film, without a noticeable loss of ¹⁶O, see Table II. The corresponding Hf signals are shown in the inset of Fig. 7. The geometry used was the same as used in previous sections. RBS revealed that hafnium amounts and the corresponding depth distribution were essentially constant for all annealing conditions and that ¹⁸O is incorporated in significantly smaller amounts than in hafnium oxide or silicate films on Si.

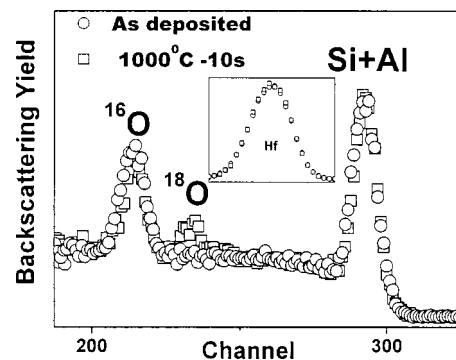


FIG. 7. Channeled-RBS spectra of 1 MeV incident He⁺, with detection of the scattered ions at 100° with the direction of incidence, from hafnium-aluminum-silicate films on Si: As-prepared sample (open circles), and after ¹⁸O₂ annealing at 1000 °C for 10 s (open squares). The corresponding Hf signals are shown in the inset.

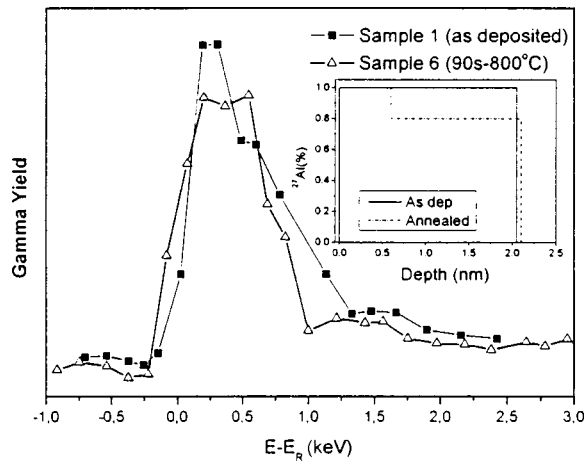


FIG. 8. Excitation curves of the $^{27}\text{Al}(p, \gamma)^{28}\text{Si}$ nuclear reaction around the resonance at 404 keV for $\text{AlHf}_x\text{Si}_y\text{O}_z$ film on Si: As-deposited sample (squares), and $^{18}\text{O}_2$ annealed at 800 °C for 90 s (triangles).

Figure 8 shows the excitation curves of the $^{27}\text{Al}(p, \gamma)^{28}\text{Si}$ reaction, corresponding to samples 1 and 6. The Al distribution is narrower than that of Si, O, and Hf, which indicates that there is a certain level of segregation of Al in the near-surface regions of the films. Slightly wider aluminum distribution is observed after annealing and there is no noticeable aluminum loss.

NNRP also shows a progressive incorporation of oxygen from the gas phase into the solid film, as shown in Fig. 9. For the lowest annealing temperatures (600 °C and 800 °C), the propagating ^{18}O front barely reaches only the $\text{AlHf}_x\text{Si}_y\text{O}_z/\text{Si}$ interface, whereas at 1000 °C a substantial amount of ^{18}O is supplied to the interface.

$\text{AlHf}_x\text{Si}_y\text{O}_z$ ultrathin films revealed to be very stable on silicon upon annealing in O_2 without dramatic changes in the

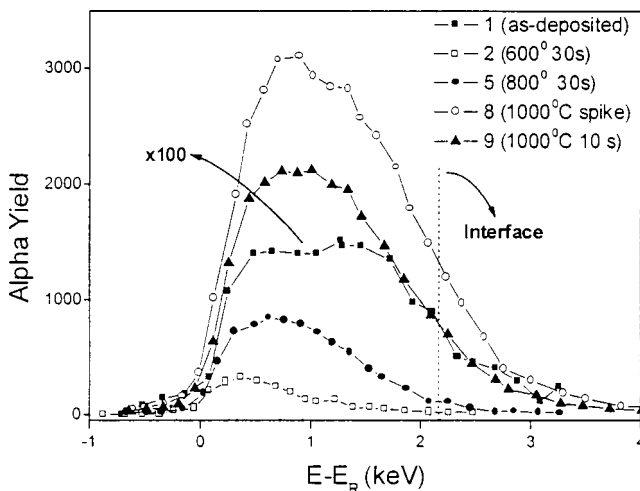


FIG. 9. Excitation curves of the $^{18}\text{O}(p, \alpha)^{15}\text{N}$ nuclear reaction around the resonance at 151 keV $\text{AlHf}_x\text{Si}_y\text{O}_z$ film on Si: As-prepared sample (solid squares, $\times 10$), annealed at 600 °C for 30 s (open squares), at 800 °C for 30 s (solid circles), at 1000 °C for 1 s (spike annealing—open circles), and annealed at 1000 °C for 10 s (solid triangles). The annealings were performed in 7×10^3 Pa of O_2 enriched to 97% in the ^{18}O isotope ($^{18}\text{O}_2$). The vertical line marks the interface position in the as-deposited sample.

composition of the films. It should be stressed here that the total amounts of oxygen from the gas phase incorporated in these films are much smaller than the corresponding ones incorporated in the hafnium oxide or hafnium–silicate films.

V. CONCLUSIONS

In summary, we have investigated the integrity and stability of HfO_2 -based ultrathin films deposited on Si, when they are submitted to typical postdeposition thermal processing used on CMOS fabrication technology.

In the case of HfO_2 films on Si, the present characterizations indicate an intermediate layer of complex composition between the room-temperature chemical vapor deposition HfO_2 films and the Si substrate, including silicon oxynitride, hafnium–silicate, and possibly hafnium–silicon oxynitride. The composition of this structure is essentially stable against Ar preannealing at 1000 °C and O_2 annealing at 800 °C. Oxygen migration proceeds by means of a propagating front from the surface that reacts with the $\text{HfO}_2/\text{SiO}_x\text{N}_y$ network as it advances, the main reaction channels being O–O and O–N exchanges.

Concerning hafnium–silicate, if one considers that RTA at 1000 °C for 30 s is sufficient for most dopant-annealing processing steps, the present results assure good integrity of amorphous films deposited by reactive sputtering on Si with a SiO_2 interlayer. Preannealing in a nonreactive atmosphere like N_2 increases the stability and resistance to oxidation of the films. Annealing in a oxygen-containing atmosphere reveals a very fast propagating front of oxygen from the film surface, which reacts with the $(\text{HfO}_2)_{1-x}(\text{SiO}_2)_x$ network as it advances. Oxygen exchange is the main reaction channel, although oxygen incorporation to complete the pseudobinary alloy stoichiometry and to oxidize a Si substrate are alternative active reaction channels. The addition of Al to hafnium–silicate, leading to Al–Hf silicates, produces dielectric films on Si that are more resistant to oxygen diffusion and incorporation.

ACKNOWLEDGMENTS

This work was partially supported by CNPq, PADCT, and FAPERGS.

¹International Technology Roadmap for Semiconductors, Semiconductor Industry Association, San Jose, California, <http://public.itrs.net> (2002).

²G. D. Wilk, R. M. Wallace, and J. M. Anthony, *J. Appl. Phys.* **87**, 484 (2000).

³B. H. Lee, L. Kang, R. Nieh, W. J. Qi, and J. C. Lee, *Appl. Phys. Lett.* **76**, 1927 (2000).

⁴A. I. Kingon, J. P. Maria, and S. K. Streiffer, *Nature (London)* **406**, 1032 (2000).

⁵C. Chaneliere, J. L. Autran, R. A. B. Devine, and B. Balland, *Mater. Sci. Eng.*, **R. 22**, 269 (1998).

⁶I. J. R. Baumvol, *Surf. Sci. Rep.* **36**, 1 (1999), and references therein.

⁷B. W. Busch, W. H. Schulte, E. Garfunkel, T. Gustafsson, W. Qi, R. Nieh, and J. Lee, *Phys. Rev. B* **62**, 13290 (2000).

⁸D. Landheer, X. Wu, J. Morais, I. J. R. Baumvol, R. P. Pezzi, L. Miotti, W. N. Lennard, and J. K. Kim, *Appl. Phys. Lett.* **79**, 2618 (2001).

⁹C. Krug, E. B. O. da Rosa, R. M. C. de Almeida, J. Morais, I. J. R. Baumvol, T. D. M. Salgado, and F. C. Stedile, *Phys. Rev. Lett.* **86**, 4714 (2001).

¹⁰M. Kundu, N. Miyata, and M. Ichikawa, *Phys. Rev. Lett.* **78**, 1517 (2001).

- ¹¹J. Morais, E. B. O. da Rosa, L. Miotti, R. P. Pezzi, I. J. R. Baumvol, A. L. P. Rotondaro, M. J. Bevan, and L. Colombo, *Appl. Phys. Lett.* **78**, 2446 (2001).
- ¹²M. R. Visokay, J. J. Chambers, A. Rotondaro, A. Shanware, and L. Colombo, *Appl. Phys. Lett.* **80**, 3183 (2002).
- ¹³S. Sayan, S. Aravamudhan, B. W. Busch, W. H. Schulte, F. Cosandey, G. D. Wilk, T. Gustafsson, and E. Garfunkel, *J. Vac. Sci. Technol. A* **20**, 507 (2002).
- ¹⁴K. J. Choi, W. C. Shin, and S. G. Yoon, *J. Electrochem. Soc.* **149**, F18 (2002).
- ¹⁵G. D. Wilk, R. M. Wallace, and J. M. Anthony, *J. Appl. Phys.* **89**, 5243 (2001).
- ¹⁶J. Morais, L. Miotti, G. V. Soares, R. P. Pezzi, S. R. Teixeira, K. P. Bastos, I. J. R. Baumvol, A. L. P. Rotondaro, M. Visokay, and L. Colombo, *Appl. Phys. Lett.* **81**, 1669 (2002).